Circular dichroism in angular distribution of electron-hydrogen scattering in a two-color bicircular laser field

Gabriela Buica*
Institute of Space Sciences, P.O. Box MG-36, Ro 77125, Bucharest-Măgurele, Romania

(Received 18 August 2018; published 21 November 2018)

We study the origin of dichroic effects in elastic scattering of high-energy electrons by hydrogen atoms in the presence of a two-color bicircular laser field of commensurate frequencies, in the domain of moderate intensities below 10 TW/cm^2. We use a semiperturbative approach in which the interaction of the hydrogen atom with the laser field is treated in second-order perturbation theory, while the interaction of the projectile electron with the laser field is described by Gordon-Volkov wave functions. An analytical formula of circular dichroism in the angular distribution of scattered electrons is derived in the weak-field domain for a two-color laser field that is a combination of the fundamental and its third harmonic. A comparison between the two-photon differential cross sections for two-color co- and counter-rotating circularly polarized laser fields is made, and the effect of the intensity ratio of the monochromatic field components on the circular dichroism is investigated. The dichroic effect in the angular distribution of scattered electrons for two-photon absorption is analyzed as a function of the scattering and azimuthal angles. We show that the two-color bicircular laser field can induce a strong circular dichroism in the angular distribution of scattered electrons at small scattering angles where the atomic dressing effects are important, as well at larger scattering angles. At small scattering angles we demonstrate that the dichroic effect for two-photon transitions can be predicted under the following conditions: the scattering process is treated in fist-order Born approximation, and the dressing of the atomic states by the laser field is carried out at least in first-order time-dependent perturbation theory.

DOI: 10.1103/PhysRevA.98.053427

I. INTRODUCTION

Dichroism, a well-known concept in classical optics, represents a property shown by certain materials of having absorption coefficients which depend on the polarization of the incident radiation [1]. In quantum mechanics the circular dichroism (CD) of an atom can be investigated by considering its interaction with circularly polarized (CP) radiation. The study of CD in laser-induced or laser-assisted atomic processes has attracted an increasing theoretical as well experimental interest in the last 30 years due to the possibility of investigating the dichroic properties of atomic systems [2–4]. Of particular interest has become the concept of circular dichroism in angular distribution (CDAD), which refers to the differences between the fluxes of scattered or ionized electrons measured at definite spatial directions, caused by left and right CP laser light [5]. One of the potential interests in dichroic measurements and calculations on laser-induced or laser-assisted atomic processes is that we can determine the relative magnitudes and phases of the various interfering transition amplitudes by analyzing the differences between the angular distributions obtained for different polarization states of the laser field [6,7]. It is interesting to note that in multiphoton ionization of unpolarized one-electron atoms by monochromatic CP light, the cross section and the angular distribution of photoelectrons do not depend on the photon helicity [8], i.e., there is no CD. However, the dichroic effect exists for two-photon ionization of atoms [6] or laser-assisted electron-atom scattering [9,10] with elliptically polarized fields. A different situation occurs in two-color photoionization of unpolarized atoms when one XUV laser beam is CP and the other near-infrared beam is linearly polarized (LP), and CDAD can exist since the angular distributions of photoelectrons are slightly different for opposite helicities of the CP field [7]. Another different situation arises when two photoelectrons are simultaneously emitted upon one-photon absorption and the angular and energy distributions of photoelectrons exhibit a strong dependence on the photon helicity [11]. Recently, the observation of CD was reported in two-color above-threshold ionization of He atoms, in both differential and integral photoelectron yield [12]. In this type of experiment the He atoms are ionized by a XUV free-electron laser radiation in the presence of an intense near-infrared laser field and the results confirmed the theoretical prediction of CD in two-color multiphoton ionization of atoms [13].

Similarly to the laser-induced processes, in laser-assisted electron-atom scattering the differential cross section (DCS) for CP light and high-energy projectiles depends neither on the dynamical phase nor on the helicity of the radiation field, in first-order Born approximation, and therefore the CD is absent [14]. However, Manakov and co-workers [15] have shown that CDAD can be predicted in laser-assisted potential scattering of low-energy electrons, provided the CP laser has low frequency and low intensity, and if the scattering amplitude is evaluated to higher orders in the Born series. In the last two decades theoretical studies of dichroic effects involving *monochromatic* electromagnetic fields, with various

*buica@spacescience.ro

combinations of linear and circular polarizations, were performed for laser-assisted electron-hydrogen scattering by Cionga and co-workers [16], in which the dressing of atomic states is taken into account in second order of time-dependent perturbation theory (TDPT). Very recently, the study of laser-assisted electron-atom scattering has attracted considerable attention, especially because of the progress of experimental techniques [17–20]. Despite the theoretical and experimental studies, the roles of the initial and final atomic states, the intermediate resonances, and the laser field parameters are still subjects of discussion. Detailed reports on the laser-assisted electron-atom collisions can be found in several review papers [21,22] and books [23,24], and references therein. A *two-color* bicircular electromagnetic field, which has lately attracted a lot of interest, consists of a superposition of two CP fields of different photon energies, which rotate in the same plane, with identical helicities (corotating CP fields) or opposite helicities (counter-rotating CP fields). The recent generation of CP high harmonics [25] allowed the direct generation of CP soft x-ray pulses and has generated an increasing attention in studying different laser-induced processes by bicircular laser fields such as strong-field ionization [26], nonsequential double ionization [27], or laser-assisted electron-ion recombination [28,29]. The physical mechanism occurring in laser-assisted or laser-induced processes involving a two-color field is the interference among different two-photon channels leading to the same final state, and obviously, by using CP fields the different helicities of the photons play an important role [30]. Obviously, the symmetries of the bicircular electromagnetic field are reflected in symmetries of the DCSs [31].

In contrast to past studies [14,16], in the present manuscript the dichroic effect is now investigated for the case of *two-color bicircular* laser fields. The notion of CDAD for two-color bicircular fields refers to the difference between DCSs of laser-assisted signals for the bichromatic fields with identical or opposite helicities [7]. To our knowledge, there are no other theoretical studies regarding the CD in laser-assisted electron-atom scattering processes in a two-color bicircular laser field which include the atomic dressing in second-order TDPT. In the present contribution we shall demonstrate that is also possible to find CDAD effects for fast electrons and small scattering angles if the dressing of the atomic states by the laser field is taken into account. Our interest is to investigate the polarization effects at UV photon energies, a domain that has not been analyzed in detail, where the atomic dressing effects are larger and, as a result the dichroic effect will be larger than at lower photon energies. Such an interest is justified because of the possibility of controlling the atomic processes by using two-color laser fields and by manipulating the photon helicity of the monochromatic components of the fields [30]. In order to avoid any complications that could mask the dichroic effect, the photon energies are chosen such that they do not match any one-photon atomic resonance. Since it is well known that the scattering probability decreases with increasing photon energy [22], we expect smaller DCSs than at lower photon energies. Therefore, we consider photon energies in the UV range (3−9 eV) and moderate laser intensities (below 10 TW/cm^2). The manuscript is organized as follows. In Sec. II we briefly present the theoretical method used in laser-assisted elastic electron-hydrogen scattering to derive the analytical formulas for the transition amplitudes for a two-color CP laser field with different polarizations [31]. As described in our previous works [32,33], a semiperturbative approach is used, in which for the interaction of the incident and scattered electrons with the laser field we employ Gordon-Volkov wave functions, while the interaction of the hydrogen atom with the laser field is treated in second-order TDPT. It is well known that the analytical studies using TDPT remain very useful for understanding essential details of the scattering signal due to the fact that the analytical formulas have the advantage of giving physical insight into the scattering process. The numerical results are discussed in Sec. III, where the DCSs and CDAD by co- and counter-rotating CP fields are analyzed as a function of the scattering and azimuthal angles of the projectile electron at different intensity ratios of the monochromatic components of the bicircular laser field. We predict a first intuitive view of the dichroic effect in the DCS and provide *simple analytic formulas*, in a closed form, of DCSs and CDAD for a bicircular field, which is a combination of a fundamental laser and its third harmonic, at low intensities or moderate intensities and large scattering angles. Finally, the summary and conclusions are given in Sec. IV. Atomic units (a.u.) are employed throughout this manuscript unless otherwise specified.

II. SEMIPERTURBATIVE THEORY

The laser-assisted *elastic scattering* of electrons by hydrogen atoms in a two-color laser field can be symbolically represented in the following way:

$$\begin{aligned} e^-(E_p,\mathbf{p}) + \mathrm{H}(1s) + N_{1i}\,\gamma(\omega_1,\boldsymbol{\varepsilon}_1) + N_{mi}\,\gamma(\omega_m,\boldsymbol{\varepsilon}_m) \\ \rightarrow e^-(E_{p'},\mathbf{p}') + \mathrm{H}(1s) + N_{1f}\,\gamma(\omega_1,\boldsymbol{\varepsilon}_1) \\ + N_{mf}\,\gamma(\omega_m,\boldsymbol{\varepsilon}_m), \end{aligned} \tag{1}$$

where $E_p\,(E_{p'})$ and $\mathbf{p}\,(\mathbf{p}')$ represent the kinetic energy and the momentum vector of the incident (scattered) projectile electron. Here $\gamma\,(\omega_k,\boldsymbol{\varepsilon}_k)$ denotes a photon with the energy ω_k and the unit polarization vector $\boldsymbol{\varepsilon}_k$, and $N_k = N_{ki} - N_{kf}$ is the net number of exchanged photons between the projectile-atom system and each monochromatic component of the two-color laser field ($k = 1$ and m). For commensurate energies, $\omega_m = m\omega_1$, the kinetic energy of the projectile electron before and after collision obeys the following conservation relation $E_{p'} = E_p + N\omega_1$, with $N \equiv N_1 + N_m\,\omega_m/\omega_1$. The two-color bicircular laser field is treated classically and is described as a combination of two coplanar CP electric fields,

$$\mathbf{E}(t) = \frac{i}{2}\sum_{k=1,m} E_{0k}\,\boldsymbol{\varepsilon}_k\,e^{-i\omega_k t} + \mathrm{c.c.}, \tag{2}$$

where E_{0k} represents the amplitude of the monochromatic components of the electric field and $\boldsymbol{\varepsilon}_1 = (\mathbf{e}_j + i\mathbf{e}_l)/\sqrt{2}$ is the polarization vector of the first laser beam, with $\mathbf{e}_j$ and $\mathbf{e}_l$ unit vectors along two orthogonal directions. The second laser beam has either the same polarization, $\boldsymbol{\varepsilon}_m = \boldsymbol{\varepsilon}_1$, for *corotating* two-color CP fields, or is circularly polarized in the opposite direction, $\boldsymbol{\varepsilon}_m = \boldsymbol{\varepsilon}_1^*$, for *counter-rotating* two-color CP fields. We use a theoretical approach similar to the one developed in Ref. [31] and, therefore, in the next sections we briefly

describe the model and approximations used to calculate DCS and CDAD.

A. Projectile electron and atomic wave functions

We assume moderate laser intensities and high-energy projectile electrons, which imply that the strength of the laser field is lower than the Coulomb field strength experienced by an electron in the first Bohr orbit, and the kinetic energy of the projectile electron is much larger than the energy of the bound electron in the first Bohr orbit [22]. We describe the initial and final states of the projectile electron interacting with a two-color laser field by Gordon-Volkov wave functions [34],

$$\chi_{\mathbf{p}}(\mathbf{r},t) = (2\pi)^{-3/2} e^{-iE_p t + i\mathbf{p}\cdot\mathbf{r} - i\mathbf{p}\cdot\boldsymbol{\alpha}_1(t) - i\mathbf{p}\cdot\boldsymbol{\alpha}_m(t)}, \tag{3}$$

where $\mathbf{r}$ is the position vector and $\boldsymbol{\alpha}_k(t)$, with $k = 1$ and m, describes the classical oscillation motion of the projectile electron in the bicircular electric fields defined by Eq. (2),

$$\boldsymbol{\alpha}_k(t) = \alpha_{0k}(\mathbf{e}_j \sin\omega_k t \pm \mathbf{e}_l \cos\omega_k t)/\sqrt{2}. \tag{4}$$

Here, the upper sign (+) is used for corotating CP fields, while the lower sign (−) is used for counter-rotating CP fields, $\alpha_{0k} = \sqrt{I_k}/\omega_k^2$ is the quiver amplitude, and $I_k = E_{0k}^2$ is the laser intensity of the monochromatic component of the two-color field. Since the calculations presented in this paper are made at moderate laser intensities, the terms proportional to the ponderomotive energy, $U_{p,k} = I_k/4\omega_k^2$, are neglected in the Gordon-Volkov wave function, Eq. (3). At a laser intensity of 1 TW/cm^2 and a photon energy of 3 eV, the ponderomotive energy is about 0.016 eV and therefore can be neglected compared to the photon and projectile energies.

The interaction of the hydrogen atom with a two-color laser field at moderate field strengths is considered within the second-order TDPT, and an approximate solution for the wave function of an electron bound to a Coulomb potential in the presence of an electric field is expressed as

$$\Psi_{1s}(\mathbf{R},t) = e^{-iE_{1s}t}\left[\psi_{1s}(\mathbf{R},t) + \psi_{1s}^{(1)}(\mathbf{R},t) + \psi_{1s}^{(2)}(\mathbf{R},t)\right], \tag{5}$$

where $\boldsymbol{R}$ denotes the position vector of the bound electron, E_{1s} is the energy of the ground state, ψ_{1s} is the unperturbed wave function of the ground state, and $\psi_{1s}^{(1)}$ and $\psi_{1s}^{(2)}$ are the first- and second-order radiative corrections to the atomic wave function. The first-order radiative correction $\psi_{1s}^{(1)}$ is calculated using the Coulomb Green's function, including both bound and continuum eigenstates, being expressed in terms of the linear-response vector [35].

Similarly, the second-order radiative correction to the atomic wave function $\psi_{1s}^{(2)}$ is expressed in terms of the quadratic response tensors [36]. For a two-color laser field, the explicit forms of the first- and second-order radiative corrections $\psi_{1s}^{(1)}$ and $\psi_{1s}^{(2)}$ are given in Ref. [31].

B. The nonlinear scattering matrix and differential cross section

As mentioned before, we focus our study at moderate laser intensities ($I_k \leqslant 10$ TW/cm^2) and fast projectile electrons ($E_p \geqslant 100$ eV) such that the interaction between the projectile electron and hydrogen atom is well treated within the first-order Born approximation in the static scattering potential $V(r,R) = -1/r + 1/|\mathbf{R} - \mathbf{r}|$. We employ a semiperturbative approach of the scattering process similar to that proposed by Byron and Joachain [37], in which the exchange scattering can be safely neglected and the scattering matrix [38] is calculated at high projectile energies as

$$S_{fi} = -i\int_{-\infty}^{+\infty} dt \langle \chi_{\mathbf{p}'}(\mathbf{r},t)\Psi_{1s}(\mathbf{R},t)|V(r,R)| \times \chi_{\mathbf{p}}(\mathbf{r},t)\Psi_{1s}(\mathbf{R},t)\rangle. \tag{6}$$

$\chi_{\mathbf{p}}$ and $\chi_{\mathbf{p}'}$ are given by Eq. (3) and represent the initial and final Gordon-Volkov wave functions of the projectile electron embedded in the two-color laser field, whereas Ψ_{1s} represents the wave function of the bound electron interacting with the two-color laser field and is calculated from Eq. (5). Using the Jacobi-Anger identity [39], $e^{ia\sin\omega t} = \sum_N J_N(a)e^{iN\omega t}$, we expand the field-dependent part of the Gordon-Volkov wave functions, $\chi_{\mathbf{p}}$ and $\chi_{\mathbf{p}'}$, in the scattering matrix in terms of the phase-dependent generalized Bessel functions B_N [40] as

$$\exp\left[-i\boldsymbol{\alpha}_1(t)\cdot\mathbf{q} - i\boldsymbol{\alpha}_m(t)\cdot\mathbf{q}\right] = \sum_{N=-\infty}^{+\infty} B_N(\mathcal{R}_1,\mathcal{R}_m;\phi_1,\phi_m)e^{-iN\omega_1 t + iN\phi_1}, \tag{7}$$

where

$$B_N(\mathcal{R}_1,\mathcal{R}_m;\phi_1,\phi_m) = \sum_{l=-\infty}^{+\infty} J_{N-ml}(\mathcal{R}_1)J_l(\mathcal{R}_m)e^{-il(m\phi_1-\phi_m)}, \tag{8}$$

in which $J_{N-ml}(\mathcal{R}_1)$ and $J_l(\mathcal{R}_m)$ are ordinary Bessel functions of the first kind. The argument of the Bessel functions of the first kind is defined by $\mathcal{R}_k = \alpha_{0k}|\boldsymbol{\varepsilon}_k\cdot\mathbf{q}|$, ($k = 1$ and m), and ϕ_k is the dynamical phase calculated as $e^{i\phi_k} = \boldsymbol{\varepsilon}_k\cdot\mathbf{q}/|\boldsymbol{\varepsilon}_k\cdot\mathbf{q}|$, where $\mathbf{q}$ denotes the momentum transfer vector of projectile during scattering, i.e., $\mathbf{q} = \mathbf{p} - \mathbf{p}'$. We note that for a monochromatic CP field with the polarization unit vector $\boldsymbol{\varepsilon}_k = (\mathbf{e}_j + i\mathbf{e}_l)/\sqrt{2}$, we obtain $\mathcal{R}_k = \alpha_{0k}\sqrt{(\mathbf{e}_j\cdot\mathbf{q})^2 + (\mathbf{e}_l\cdot\mathbf{q})^2}/\sqrt{2}$ and $\phi_k = \arctan(\mathbf{e}_l\cdot\mathbf{q})/(\mathbf{e}_j\cdot\mathbf{q}) + s\pi$, where s is an integer. Clearly, a change of helicity of the CP field, i.e., $\boldsymbol{\varepsilon}_k \to \boldsymbol{\varepsilon}_k^*$, leads to a change of the sign of the dynamical phase, $\phi_k \to -\phi_k$. By replacing Eqs. (3), (5), and (7) in Eq. (6), we obtain, after integrating over time and over projectile coordinate, the scattering matrix for elastic electron-hydrogen collisions in a two-color laser field,

$$S_{fi} = -2\pi i\sum_{N=-\infty}^{+\infty} T_{fi,N}\,\delta(E_{p'} - E_p - N\omega_1), \tag{9}$$

where in the δ Dirac function the kinetic energy of the projectile is modified by $N\omega_1$. Hence, the energy spectrum of the scattered electron consists of an elastic line $N = 0$ ($E_{p'} = E_p$ and $N_{ki} = N_{kf}$), and of a number of sidebands corresponding to the positive and negative values of N. The total nonlinear transition amplitude $T_{fi,N}$ for the elastic scattering process is expressed as a sum of three terms,

$$T_{fi,N} = T_N^{(0)} + T_N^{(1)} + T_N^{(2)}, \tag{10}$$

and the nonlinear DCS of the scattered electrons is calculated as

$$\frac{d\sigma_N}{d\Omega_{p'}} = (2\pi)^4 \frac{p'}{p} \left| T_N^{(0)} + T_N^{(1)} + T_N^{(2)} \right|^2, \tag{11}$$

where the final momentum of the projectile is given by $p' = (p^2 + 2N\omega_1)^{1/2}$.

The derivation of the transition amplitudes $T_N^{(i)}$, $(i = 0, 1, 2)$, is briefly described in what follows. The first term on the right-hand side of the total transition amplitude Eq. (10), $T_N^{(0)}$, is the elastic transition amplitude due to projectile electron contribution in which the atomic dressing is neglected,

$$T_N^{(0)} = B_N(\mathcal{R}_1, \mathcal{R}_m; \phi_1, \phi_m) F(\mathbf{q}), \tag{12}$$

where the atomic form factor is given by $F(\mathbf{q}) = (2\pi^2 q^2)^{-1} \langle \psi_{1s} | e^{i\mathbf{q}\cdot\mathbf{R}} - 1 | \psi_{1s} \rangle$. After performing the radial integration in the atomic form factor, we obtain the electronic transition amplitude

$$T_N^{(0)} = -\frac{1}{(2\pi)^2} B_N(\mathcal{R}_1, \mathcal{R}_m; \phi_1, \phi_m)\, f_{el}^{B_1}(q), \tag{13}$$

in which $f_{el}^{B_1}(q) = 2(q^2 + 8)/(q^2 + 4)^2$ is the first-order Born approximation of the scattering amplitude for the elastic scattering process in the absence of the laser field. The laser field dependence is contained in the arguments of the generalized Bessel function only $B_N(\mathcal{R}_1, \mathcal{R}_m; \phi_1, \phi_m)$.

The second term on the right-hand side of Eq. (10), $T_N^{(1)}$, represents the first-order atomic transition amplitude and occurs due to modification of the atomic ground state by the two-color laser field (*atomic dressing*), which is described by the first-order radiative correction, $\psi_{1s}^{(1)}(\mathbf{R}, t)$. After some calculation, the first-order atomic transition amplitude can be written as

$$T_N^{(1)} = -\sum_{k=1,m} \frac{\alpha_{0k}\omega_k}{2} \big[B_{N-k}\, \mathcal{M}_{at}^{(1)}(\omega_k, \mathbf{q}) e^{-ik\phi_1} + B_{N+k}\, \mathcal{M}_{at}^{(1)}(-\omega_k, \mathbf{q}) e^{ik\phi_1} \big], \tag{14}$$

where $\mathcal{M}_{at}^{(1)}(\omega_k, \mathbf{q})$ denotes specific first-order atomic transition matrix elements related to one-photon absorption, whereas the transition matrix elements $\mathcal{M}_{at}^{(1)}(-\omega_k, \mathbf{q})$ are related to one-photon emission [31]. Obviously, in Eq. (14) only one photon is exchanged (emitted or absorbed) between the two-color laser and the bound electron, while the remaining $N \pm 1$ photons are exchanged between the two-color laser and the projectile electron. For the sake of simplicity, the arguments of the generalized Bessel functions are dropped off in Eq. (14) and throughout this paper. By performing the radial integrals in Eq. (14) we find the first-order atomic transition amplitude $T_N^{(1)}$ as

$$T_N^{(1)} = \sum_{k=1,m} \frac{\alpha_{0k}\omega_k}{4\pi^2 q^2} [(\boldsymbol{\varepsilon}_k \cdot \hat{\mathbf{q}}) B_{N-k} \mathcal{J}_{101}(\omega_k, q) e^{-ik\phi_1} - (\boldsymbol{\varepsilon}_k^* \cdot \hat{\mathbf{q}}) B_{N+k} \mathcal{J}_{101}(\omega_k, q) e^{ik\phi_1}], \tag{15}$$

where the radial integral $\mathcal{J}_{101}(\omega_k, q)$ is analytically calculated as a series of hypergeometric functions [14,32], and $\hat{\mathbf{q}} = \mathbf{q}/|\mathbf{q}|$ represents a unit vector that defines the direction of the momentum transfer vector.

The last term on the right-hand side of the transition amplitude Eq. (10), $T_N^{(2)}$, represents the second-order atomic transition amplitude and occurs due to alteration of the atomic ground state by the two-color laser field, which is described by the second-order radiative correction $\psi_{1s}^{(2)}(\mathbf{R}, t)$, calculated in Ref. [31]. After some algebra the second-order atomic transition amplitude $T_N^{(2)}$ is expressed as

$$T_N^{(2)} = \sum_{k=1,m} \frac{\alpha_{0k}^2 \omega_k^2}{4} \big\{ B_{N-2k} \mathcal{M}_{at}^{(2)}(\omega_k, \mathbf{q}) e^{-2ik\phi_1} + B_{N+2k} \mathcal{M}_{at}^{(2)}(-\omega_k, \mathbf{q}) e^{2ik\phi_1} + B_N \big[\widetilde{\mathcal{M}}_{at}^{(2)}(E_{1s}, \omega_k) + \widetilde{\mathcal{M}}_{at}^{(2)}(E_{1s}, -\omega_k) \big] \big\} + \frac{\alpha_{01}\alpha_{0m}\omega_1\omega_m}{4} \sum_{l,j=\pm 1} B_{N-l-jm} \mathcal{N}_{at}^{(2)}(l\omega_1, j\omega_m, \mathbf{q}) e^{-i(l+jm)\phi_1}. \tag{16}$$

Obviously, in Eq. (16) only two photons are exchanged (absorbed, emitted, or absorbed and emitted) between the two-color laser field and the bound electron. The specific second-order atomic transition matrix elements, $\mathcal{M}_{at}^{(2)}$, $\widetilde{\mathcal{M}}_{at}^{(2)}$, and $\mathcal{N}_{at}^{(2)}$, are connected to two-photon exchange and are calculated in Refs. [14,41]. The atomic transition matrix elements $\mathcal{M}_{at}^{(2)}(\omega_k, \mathbf{q})$ and $\mathcal{M}_{at}^{(2)}(-\omega_k, \mathbf{q})$ are related to absorption and emission of two identical photons of energy ω_k and complex polarization $\boldsymbol{\varepsilon}_k$, respectively. The second type of atomic transition matrix elements $\widetilde{\mathcal{M}}_{at}^{(2)}(\omega_k, \mathbf{q})$ describe the absorption followed by emission of the same photon, whereas $\widetilde{\mathcal{M}}_{at}^{(2)}(-\omega_k, \mathbf{q})$ describes the emission followed by absorption of the same photon. The third type of atomic transition matrix elements $\mathcal{N}_{at}^{(2)}(\omega_1, \omega_m, \mathbf{q})$ and $\mathcal{N}_{at}^{(2)}(-\omega_1, -\omega_m, \mathbf{q})$ describe the absorption and emission of two different photons of energies ω_1 and ω_m, respectively. Similarly, $\mathcal{N}_{at}^{(2)}(-\omega_1, \omega_m, \mathbf{q})$ are related to emission of one photon of energy ω_1 and absorption of one photon of energy ω_m. The analytic expressions of the second-order atomic transition matrix elements for two *identical* photons are given by

$$\mathcal{M}_{at}^{(2)}(\omega_k, \mathbf{q}) = \frac{(\boldsymbol{\varepsilon}_k \cdot \hat{\mathbf{q}})^2}{2\pi^2 q^2} \mathcal{Q}(\omega_k, q) + \frac{\boldsymbol{\varepsilon}_k^2}{2\pi^2 q^2} \mathcal{P}(\omega_k, q) \tag{17}$$

and

$$\widetilde{\mathcal{M}}_{at}^{(2)}(\omega_k, \mathbf{q}) = \frac{|\boldsymbol{\varepsilon}_k \cdot \hat{\mathbf{q}}|^2}{2\pi^2 q^2} \widetilde{\mathcal{Q}}(\omega_k, q) + \frac{1}{2\pi^2 q^2} \widetilde{\mathcal{P}}(\omega_k, q), \tag{18}$$

where the specific expressions of the polarization-invariant atomic radial integrals $\mathcal{P}$ and $\mathcal{Q}$ for two-photon processes depend on the photon energies and the amplitude of the momentum transfer vector of the projectile electron, and are obtained as series of hypergeometric functions in Ref. [14]. We note that $\boldsymbol{\varepsilon}_k^2 = 1$ for a LP field, while $\boldsymbol{\varepsilon}_k^2 = 0$ for a CP field and therefore, the second term in the right-hand side of Eq. (17) vanishes.

For the exchange of two *different* photons, a general form of the second-order atomic transition matrix elements was derived [41] as

$$\mathcal{M}_{at}^{(2)}(\omega_j, \omega_l, \mathbf{q}) = \frac{(\boldsymbol{\varepsilon}_j \cdot \hat{\mathbf{q}})(\boldsymbol{\varepsilon}_l \cdot \hat{\mathbf{q}})}{2\pi^2 q^2} \mathcal{Q}'(\omega_j, \omega_l, q) + \frac{\boldsymbol{\varepsilon}_j \cdot \boldsymbol{\varepsilon}_l}{2\pi^2 q^2} \mathcal{P}'(\omega_j, \omega_l, q). \tag{19}$$

Equation (19) is symmetric and has a structure that explicitly contains only the scalar products of polarization and momentum transfer vectors. The general structure of Eq. (19) is also similar to other processes, such as the elastic scattering of photons by hydrogen atoms [42], two-photon bremsstrahlung [43], elastic x-ray scattering by ground-state atoms [44], two-photon ionization of hydrogen [7,45], or two-photon double ionization [46], with the unit vector $\hat{\mathbf{q}}$ replaced by vectors which are specific to each particular process. The specific expressions of the polarization-invariant atomic radial integrals for two different photons, $\mathcal{P}'$ and $\mathcal{Q}'$, depend on the photon energies ω_j and ω_l, and the momentum transfer q [41]. The following the changes are made, $\omega_k \to -\omega_k$ and $\boldsymbol{\varepsilon}_k \to \boldsymbol{\varepsilon}_k^*$, if the photon k is emitted ($k = j$ and l). Clearly, for the absorption of two distinct photons with identical circular polarizations $\boldsymbol{\varepsilon}_j = \boldsymbol{\varepsilon}_l$ (corotating CP fields) the second term on the right-hand side of Eq. (19) vanishes, while for opposite polarizations $\boldsymbol{\varepsilon}_l = \boldsymbol{\varepsilon}_j^*$ (counter-rotating CP fields) we have $\boldsymbol{\varepsilon}_j \cdot \boldsymbol{\varepsilon}_l = 1$.

Finally, the CDAD is defined as the difference between the laser-assisted DCSs for co- and counter-rotating two-color CP fields,

$$\Delta_{CDAD}(\theta, \varphi) = \frac{d\sigma_N^{++}}{d\Omega_{p'}}(\theta, \varphi) - \frac{d\sigma_N^{+-}}{d\Omega_{p'}}(\theta, \varphi), \tag{20}$$

where the superscript $++$ indicates that both monochromatic components of the field have identical polarizations (corotating fields), while superscript $+-$ indicates that the monochromatic components have opposite polarizations (counter-rotating fields). It is interesting to note that the explicit or implicit presence of the dynamical phase factors $e^{i\phi_l}$ and $e^{i\phi_m}$ in the electronic as well the first- and second-order atomic transitions amplitudes, Eqs. (13), (15), and (16), can give different interference terms in the expression of DCS for corotating in comparison to counter-rotating CP fields.

For practical reasons the circular dichroism in angular distribution can be better visualized through a relative CDAD, defined as the ratio between the difference of DCSs for corotating and counter-rotating fields and the sum of these DCSs,

$$R(\theta, \phi) = \Delta_{CDAD}(\theta, \varphi) \left[\frac{d\sigma_N^{++}}{d\Omega_{p'}}(\theta, \varphi) + \frac{d\sigma_N^{+-}}{d\Omega_{p'}}(\theta, \varphi) \right]^{-1}. \tag{21}$$

Obviously, the relative CDAD defined in the above equation approaches values of $+1$ or -1 in those cases where one of the DCSs, $d\sigma_N^{++}/d\Omega_{p'}$ or $d\sigma_N^{+-}/d\Omega_{p'}$, is almost equal to zero, whereas the relative CDAD approaches the value zero in those cases where $d\sigma_N^{++}/d\Omega_{p'} \simeq d\sigma_N^{+-}/d\Omega_{p'}$.

III. NUMERICAL EXAMPLES AND DISCUSSION

In this section, we present numerical results for the scattering process described by Eq. (1), in which two photons are absorbed in the electron-hydrogen scattering process embedded in a two-color CP laser, which is a combination of the fundamental and its third harmonic ($m = 3$). It is worth pointing out that Eqs. (13), (15), and (16) are applicable for arbitrary scattering configurations and two-color laser fields with linear and/or circular polarizations. We focus our discussion on two different polarizations where the two-color laser beams are CP in the (x, y) plane with one laser beam propagating in the z-axis direction, $\boldsymbol{\varepsilon}_1 = \boldsymbol{\varepsilon}_+ \equiv (\mathbf{e}_x + i\mathbf{e}_y)/\sqrt{2}$ (left-handed CP), while the other laser beam has either the same circular polarization $\boldsymbol{\varepsilon}_3 = \boldsymbol{\varepsilon}_+$, i.e., the *corotating polarization* case, or is CP in the opposite direction, $\boldsymbol{\varepsilon}_3 = \boldsymbol{\varepsilon}_- \equiv (\mathbf{e}_x - i\mathbf{e}_y)/\sqrt{2}$ (right-handed CP), i.e., *counter-rotating polarization* case. For example, in the case of equal amplitudes of the monochromatic field components ($E_{01} = E_{03}$), the bicircular electric field defined in Eq. (2) reduces to

$$\mathbf{E}_+(t) = E_{01}\sqrt{2}\,(\mathbf{e}_x \sin\omega_+ t - \mathbf{e}_y \cos\omega_+ t)\cos\omega_- t, \tag{22}$$

for identical circular polarizations ($\boldsymbol{\varepsilon}_1 = \boldsymbol{\varepsilon}_3 = \boldsymbol{\varepsilon}_+$), and

$$\mathbf{E}_-(t) = E_{01}\sqrt{2}\,(\mathbf{e}_x \cos\omega_- t - \mathbf{e}_y \sin\omega_- t)\sin\omega_+ t, \tag{23}$$

for opposite circular polarizations ($\boldsymbol{\varepsilon}_1 = \boldsymbol{\varepsilon}_+$ and $\boldsymbol{\varepsilon}_3 = \boldsymbol{\varepsilon}_-$), where the frequencies are defined by $\omega_\pm = \eta\,\omega_1/2$, with $\eta = 2$ for corotating CP fields and $\eta = 4$ for counter-rotating CP fields. The bicircular electric field vectors, Eqs. (22) and (23), are invariant with respect to translation in time by an integer multiple of T_1/η and with respect to rotation in the polarization plane by an angle $\alpha = 2\pi/\eta$ around the z axis, such that $\mathbf{E}_\pm(t + T_1/\eta) = \boldsymbol{R}(2\pi/\eta)\,\mathbf{E}_\pm(t)$, where $\boldsymbol{R}(\alpha)$ is a 2×2 rotation matrix with angle α around the z axis and $T_1 = 2\pi/\omega_1$ is the fundamental field optical period.

In Fig. 1 we plot the temporal dependence of the electric field vectors, given by Eqs. (22) and (23), in the polarization plane for two-color CP laser fields of equal intensities with identical polarizations in the right column and opposite polarizations in the left column. For counter-rotating polarizations the temporal symmetry of the electric field means that $\mathbf{E}_-(t + T_1/4) = \boldsymbol{R}(\pi/2)\,\mathbf{E}_-(t)$, i.e., the translation in time is one-quarter of the optical cycle, $T_1/4$, and the rotation angle in the polarization plane is $\pi/2$, which implies a fourfold symmetry of the electric field in Fig. 1(a). By contrast, for corotating polarizations the translation in time of the electric field is $T_1/2$ and the rotation angle is π in Fig. 1(b), such that $\mathbf{E}_+(t + T_1/2) = \boldsymbol{R}(\pi)\,\mathbf{E}_+(t)$. We expect the symmetries of the bicircular field to be preserved in the DCSs of the scattered electron. The laser intensities we consider in Fig. 1 are $I_1 = I_3 = 1$ TW/cm^2, and the fundamental and harmonic photon energies are $\omega_1 = 3$ eV and $\omega_3 = 9$ eV.

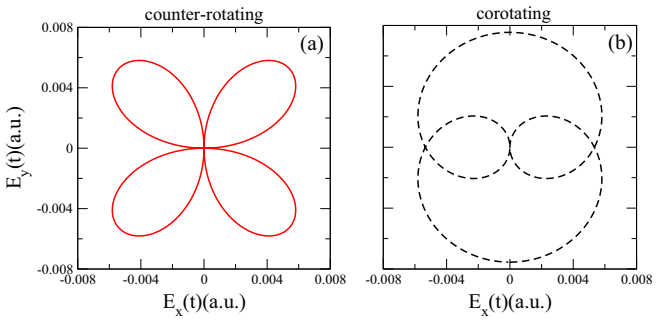

FIG. 1. Parametric plots showing the Cartesian components of the electric field vector in the (x, y)-polarization plane, $E_x(t)$ and $E_y(t)$, plotted for $0 \leqslant t \leqslant T_1$, for two-color left- and right-handed CP fields with $\boldsymbol{\varepsilon}_1 = \boldsymbol{\varepsilon}_+ = (\mathbf{e}_x + i\mathbf{e}_y)/\sqrt{2}$ and $\boldsymbol{\varepsilon}_3 = \boldsymbol{\varepsilon}_-$ in panel (a), and two-color left-handed CP fields with $\boldsymbol{\varepsilon}_1 = \boldsymbol{\varepsilon}_3 = \boldsymbol{\varepsilon}_+$ in panel (b). The laser field intensities are $I_1 = I_3 = 1$ TW/cm^2, the fundamental photon energy is $\omega_1 = 3$ eV, while the energy of the harmonic photon is $\omega_3 = 3\omega_1$. The two-color bicircular electric field satisfies a $T_1/2$ and $T_1/4$ rotational symmetry for co- and counter-rotating polarizations, respectively.

A. Two-photon circular dichroism in a weak bicircular laser field

In this section we derive simple analytical formulas of nonlinear DCSs and CDAD for two-photon absorption in the weak-laser-field regime, which provide more physical insight into the dichroic effect in the electron-hydrogen scattering process in a two-color bicircular laser field. The total transition amplitude that includes the first- and second-order atomic dressing can be written in a closed form that allows us to analyze the dependence on the polarization vectors. In what follows we consider the scattering geometry depicted in Fig. 2 in which the momentum vector of the incident electron $\mathbf{p}$ is parallel to the z axis, θ is the scattering angle between the momentum vectors of the incident and scattered

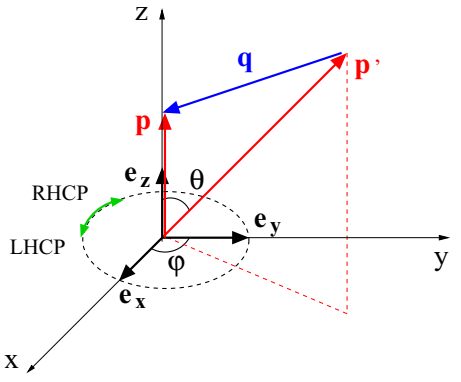

FIG. 2. The specific scattering geometry with $\mathbf{p} \parallel \mathbf{e}_z$, where $\mathbf{p}$ and $\mathbf{p}'$ are the momentum vectors of the incident and scattered electron, θ is the angle between them, φ is the azimuthal angle, and $\mathbf{q}$ is the momentum transfer vector. We assume that both laser beams are collinear and propagate along the Oz axis. The laser beams are CP in the (x, y) plane, with the polarization vectors $\boldsymbol{\varepsilon}_+ = (\mathbf{e}_x + i\mathbf{e}_y)/\sqrt{2}$ left-handed CP (LHCP) or $\boldsymbol{\varepsilon}_- = (\mathbf{e}_x - i\mathbf{e}_y)/\sqrt{2}$ right-handed CP (RHCP).

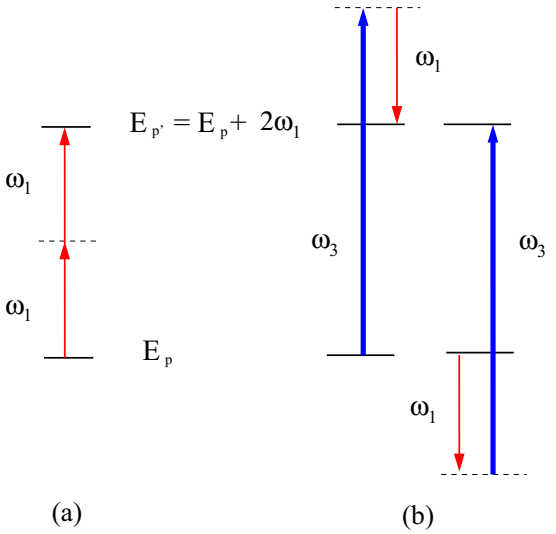

FIG. 3. Energy diagrams schematically showing the photon channels leading to the final energy of the projectile electron $E_{p'} = E_p + 2\omega_1$. Channel (a) corresponds to absorption of two photons of energy ω_1, while channel (b) corresponds to absorption of one third-harmonic photon $\omega_3 = 3\omega_1$ and emission of one photon ω_1.

electrons $\mathbf{p}$ and $\mathbf{p}'$, and φ is the azimuthal angle of the scattered electron. In this scattering geometry the Cartesian components of the momentum transfer vector $\mathbf{q}$ are given by $(-p'\sin\theta\cos\varphi, -p'\sin\theta\sin\varphi, p - p'\cos\theta)$, with an amplitude $q = \sqrt{p'^2 + p^2 - 2p'p\cos\theta}$ which varies in the interval $|p' - p| \leqslant q \leqslant p' + p$, for forward ($\theta = 0^\circ$) and backward ($\theta = 180^\circ$) scattering, where $p' = \sqrt{p^2 + 2N\omega_1}$. Whenever the arguments of the Bessel function of the first kind are small, i.e., $\mathcal{R}_1 \ll 1$ and $\mathcal{R}_3 \ll 1$, a condition that is satisfied either at low laser intensities or at small scattering angles with moderate laser intensities, the approximate expressions of the generalized Bessel functions can be used [31,39]. Hence, in the limit $\mathcal{R}_{1(3)} \ll 1$ the total transition amplitude for two-photon absorption is calculated by keeping the second-order contributions in the fields and neglecting the higher powers of the fields in Eqs. (13), (15), and (16) as a sum of the two-photon transition amplitudes for the channels depicted in Fig. 3,

$$T_2 \simeq \alpha_{01}^2 |\boldsymbol{\varepsilon}_1 \cdot \mathbf{q}|^2 \mathcal{C}_1 + \alpha_{01}\alpha_{03} |\boldsymbol{\varepsilon}_1^* \cdot \mathbf{q}| |\boldsymbol{\varepsilon}_3 \cdot \mathbf{q}| \mathcal{C}_2 \, e^{-i(3\phi_1 - \phi_3)} + \alpha_{01}\alpha_{03} (\boldsymbol{\varepsilon}_1^* \cdot \boldsymbol{\varepsilon}_3) \mathcal{C}_3 \, e^{-2i\phi_1}. \tag{24}$$

The first term on the right-hand side describes absorption of two identical photons of energy ω_1, while the rest of the terms describe absorption of one photon of energy ω_3 and emission of another photon of energy ω_1, as schematically presented in Figs. 3(a) and 3(b). The polarization-invariant amplitudes $\mathcal{C}_1$, $\mathcal{C}_2$, and $\mathcal{C}_3$ depend on the momentum transfer and photon energies being defined as

$$\mathcal{C}_1 = \frac{1}{8\pi^2}\left[-\frac{f_{el}^{B_1}}{4} + \frac{\omega_1}{q^3}\mathcal{J}_{101}(\omega_1, q)\right], \tag{25}$$

$$\mathcal{C}_2 = \frac{1}{8\pi^2}\left[\frac{f_{el}^{B_1}}{2} - \frac{\omega_3}{q^3}\mathcal{J}_{101}(\omega_3, q) + \frac{\omega_1\omega_3}{q^4}\mathcal{Q}'(-\omega_1, \omega_3, q)\right], \tag{26}$$

$$\mathcal{C}_3 = \frac{\omega_1\omega_3}{8\pi^2 q^2}\mathcal{P}'(-\omega_1, \omega_3, q). \tag{27}$$

In the scattering geometry shown in Fig. 2, the scalar product in the argument $\mathcal{R}_k$ of the generalized Bessel functions is given by $\boldsymbol{\varepsilon}_\pm \cdot \mathbf{q} = -p' \sin\theta\, e^{\pm i\varphi}/\sqrt{2}$ and the dynamical phases of the corotating laser fields are $\phi_1 = \phi_3 = \pi + \varphi$, whereas for counter-rotating laser fields only the dynamical phase of the harmonic field changes as $\phi_3 = \pi - \varphi$. Obviously, a change of the photon helicity in the arguments of the generalized Bessel functions implies a change in the sign of the azimuthal angle φ. Therefore, in the weak-field limit of a two-color bicircular laser, with $\boldsymbol{\varepsilon}_3 = \boldsymbol{\varepsilon}_+$ for the corotating case and $\boldsymbol{\varepsilon}_3 = \boldsymbol{\varepsilon}_-$ for the counter-rotating case, we obtain the following two-photon transition amplitude:

$$T_2 \simeq \alpha_{01}^2 |\boldsymbol{\varepsilon}_1 \cdot \mathbf{q}|^2 \left(\mathcal{C}_1 + \frac{\alpha_{03}}{\alpha_{01}}\mathcal{C}_2\, e^{-i\eta\varphi}\right) + \delta_{2\eta}\, \alpha_{01}\alpha_{03}\, \mathcal{C}_3\, e^{-2i\varphi}, \tag{28}$$

where the parameter η is either 2 for two-color corotating CP fields (equal photon helicities) or 4 for two-color counter-rotating CP fields (opposite photon helicities), respectively. After substituting the scalar product $|\boldsymbol{\varepsilon}_1 \cdot \mathbf{q}|$ in the above equation the corresponding two-photon DCSs in a weak bicircular laser field for co- and counter-rotating polarizations take the following simple forms:

$$\frac{d\sigma_2^{++}}{d\Omega_{p'}}(\theta, \varphi) \simeq |a_1 \sin^2\theta + (a_2 \sin^2\theta + a_3)e^{-2i\varphi}|^2, \tag{29}$$

$$\frac{d\sigma_2^{+-}}{d\Omega_{p'}}(\theta, \varphi) \simeq |a_1 + a_2 e^{-4i\varphi}|^2 \sin^4\theta, \tag{30}$$

with $a_1 = 2\pi^2\alpha_{01}^2\mathcal{C}_1\sqrt{p'^3/p}$, $a_2 = 2\pi^2\alpha_{01}\alpha_{03}\,\mathcal{C}_2\sqrt{p'^3/p}$, and $a_3 = 4\pi^2\alpha_{01}\alpha_{03}\,\mathcal{C}_3\sqrt{p'/p}$. Clearly, the co- and counter-rotating DCSs, $d\sigma_2^{++}/d\Omega_{p'}$ and $d\sigma_2^{+-}/d\Omega_{p'}$, are different for opposite helicities of the CP harmonic laser field.

Finally, the two-photon CDAD defined by Eq. (20) is simply calculated in the weak bicircular laser field limit as the difference between the DCSs given by Eqs. (29) and (30),

$$\Delta_{CDAD}(\theta, \varphi) \simeq |a_3|^2 + 2\mathrm{Re}\,[a_2 a_3^* \sin^2\theta + a_1^* \sin^2\theta(a_2 \sin^2\theta + a_3)e^{-2i\varphi} - a_1^* a_2 \sin^4\theta e^{-4i\varphi}]. \tag{31}$$

Furthermore, as long as the harmonic photon energy is below the ionization threshold, $\omega_1 < |E_{1s}|/3$, the one- and two-photon atomic transition matrix elements $\mathcal{M}_{at}^{(1)}$, $\mathcal{M}_{at}^{(2)}$, and $\mathcal{N}_{at}^{(2)}$ are real quantities. Therefore, CDAD can be formally expressed from Eq. (31) as a function of the scattering and azimuthal angles θ and φ,

$$\Delta_{CDAD}(\theta, \varphi) \simeq a_3(a_3 + 2a_2 \sin^2\theta) + 2a_1 \sin^2\theta(a_2 \sin^2\theta + a_3)\cos(2\varphi) - 2a_1 a_2 \sin^4\theta \cos(4\varphi). \tag{32}$$

Excepting the forward and backward scattering where CDAD is φ independent, the last two terms in the right-hand side depend on $\cos(2\varphi)$ and $\cos(4\varphi)$. CDAD is invariant to the following transformations: (i) $\pi - \varphi \to \pi + \varphi$, which is equivalent to a reflection with respect to the (x, z) plane, and (ii) $\pi/2 - \varphi \to \pi/2 + \varphi$, which is equivalent to a reflection with respect to the (y, z) plane. According to Eq. (32) the dichroic effect can be encountered even for rather small scattering angles where the atomic dressing is important, not only around the scattering angle $\theta = 90^\circ$ as in the case of x-ray scattering by unoriented systems [44], or the case of two-color two-photon photoionization when the polarization state of one of the fields is reversed [7]. Obviously, as was previously mentioned, in first-order Born approximation the dichroic effect in DCS cannot be encountered in a scattering configuration involving only a *one-color* (ω_1) CP laser field [14,15], because the two-photon transition amplitude given by Eq. (24) does not depend on the helicity of the radiation field. However, a dichroic effect in two-photon transitions can be predicted for a superposition of one-color LP and CP fields under the following conditions: the scattering of the high-energy electrons is treated in the first-order Born approximation, the atomic dressing effect by the laser field is carried out in second-order TDPT, and the transitions between the atomic bound and continuum states are energetically allowed [16]. In contrast to the findings of Ref. [16], our Eq. (32) shows a different regime were the dichroic effect in DCS is encountered for a two-color bicircular laser field even if the atomic dressing is neglected or the photon energies are below the ionization threshold, such that $\omega_1 + \omega_3 < |E_{1s}|$. In addition, if the atomic dressing is small in Eqs. (25), (26), and (27), i.e., at large scattering angles with nonresonant photon energies or in the limit of low-photon energies, i.e., $E_p \gg \omega_1$, by keeping the first-order dressing in fields $\mathcal{J}_{101}(\omega, q) \simeq \alpha_d\, \omega\, q$ [14], $\mathcal{P} \simeq 0$, and $\mathcal{Q} \simeq 0$, we obtain

$$a_1 = \frac{\alpha_{01}^2}{4}\sqrt{\frac{p'^3}{p}}\left(\alpha_d \frac{\omega_1^2}{q^2} - \frac{f_{el}^{B_1}}{4}\right), \tag{33}$$

$$a_2 = \frac{\alpha_{01}\alpha_{03}}{4}\sqrt{\frac{p'^3}{p}}\left(\frac{f_{el}^{B_1}}{2} - \alpha_d \frac{\omega_3^2}{q^2}\right), \tag{34}$$

$$a_3 = 0, \tag{35}$$

where α_d is the dynamic dipole polarizability of the hydrogen atom in its ground state. For high projectile energies and low photon energies, $p' \simeq p$, the projectile momentum transfer has a simple dependence on the scattering angle θ and the following approximation formula holds for momentum transfer: $q \simeq p \sin(\theta/2)$. Therefore, the CDAD is then simply expressed as

$$\Delta_{CDAD}(\theta, \varphi) \simeq 4a_1 a_2 \sin^4\theta \sin(\varphi)\sin(3\varphi), \tag{36}$$

and the relative CDAD is formally calculated as

$$R_{CDAD}(\theta, \varphi) \simeq \frac{2a_1 a_2 \sin(\varphi)\sin(3\varphi)}{a_1^2 + a_2^2 + 2a_1 a_2 \cos(\varphi)\cos(3\varphi)}. \tag{37}$$

Both Δ_{CDAD} and R_{CDAD} vanish at azimuthal angles that are multiples of $\pi/3$. Their absolute maxima occur at azimuthal angles $\pi/2$ and $3\pi/2$, while their minima occur

at $s\pi \pm \arccos(0.25)/2$, where s is an integer. The maximum of the dichroic effect in the weak-laser-field domain is found from Eqs. (36) and (37) for an optimal laser intensity ratio $I_3/I_1 \simeq 20.2$, where $a_1 \simeq a_2$ and $R_{CDAD}(\theta,\varphi) \simeq \sin(\varphi)\sin(3\varphi)/[1+\cos(\varphi)\cos(3\varphi)]$. Therefore, the advantage of analyzing the relative difference between the angular distributions obtained for two-color co- and counter-rotating CP fields, Eq. (37), is that we can determine the relative magnitude, a_1/a_2, of the interfering transition amplitudes.

B. Two-photon circular dichroism at moderate laser intensity

Now we apply the semiperturbative formulas derived in Sec. II, Eqs. (12), (14), and (16), to evaluate numerically the nonlinear DCSs and CDAD for two-photon absorption ($N = 2$) in elastic electron scattering by a hydrogen atom in the presence of two-color co- and counter-rotating CP laser fields. We have chosen moderate laser intensities below 10 TW/cm^2, a high energy of the projectile electron $E_p = 100$ eV, and photon energies in the UV range $\omega_1 = 3$ eV and $\omega_3 = 9$ eV, such that neither the projectile electron nor the photon can separately excite an upper atomic state. The polarization vectors of the two-color bicircular laser field are given by $\boldsymbol{\varepsilon}_1 = (\mathbf{e}_x + i\mathbf{e}_y)/\sqrt{2}$ and $\boldsymbol{\varepsilon}_3 = \boldsymbol{\varepsilon}_1$ for the corotating case, and $\boldsymbol{\varepsilon}_1 = (\mathbf{e}_x + i\mathbf{e}_y)/\sqrt{2}$ and $\boldsymbol{\varepsilon}_3 = (\mathbf{e}_x - i\mathbf{e}_y)/\sqrt{2}$ for the counter-rotating case.

To start with a simple case, we present in Fig. 4 our numerical results for the three-dimensional DCSs, projected in the polarization plane, as a function of the normalized projectile momentum p'_x/p' and p'_y/p' for (a) two-color left-handed CP field (corotating) in the right column and (b) left- and right-handed CP fields (counter-rotating) in the left column. The intensities of the fundamental and third-harmonic laser are considered equal, as $I_1 = I_3 = 1$ TW/cm^2, which result in a quiver motion amplitude $\alpha_{01} \simeq 0.44$ a.u. and an argument of the Bessel function $\mathcal{R}_1 \simeq 0.44|\boldsymbol{\varepsilon}_1 \cdot \mathbf{q}|$ for the fundamental field, while for the harmonic field the corresponding parameters α_{03} and $\mathcal{R}_3$ are 9 times smaller. At laser intensities higher than 10 TW/cm^2 the multiphoton ionization becomes a competing process and should be taken into account. The total DCS, the projectile contribution to DCS calculated as $(2\pi)^4(p'/p)|T_2^{(0)}|^2$, Eq. (12), and the first- and second-order atomic dressing contributions calculated as $(2\pi)^4(p'/p)|T_2^{(1)}|^2$ and $(2\pi)^4(p'/p)|T_2^{(2)}|^2$, Eqs. (14) and (16), are shown from top to bottom in Fig. 4. The first- and second-order atomic contributions to DCSs, i.e., the last two rows in Fig. 4, give significant contributions at relatively small scattering angles $\theta < 30^\circ$, while the projectile electron contribution, i.e., the second row in Fig. 4, gives important contributions at larger scattering angles. It is clear that at small scattering angles the differences between the co- and counter-rotating DCSs originate from the different first- and second-order atomic dressing, whereas at large scattering angles the differences come from the different projectile electron contributions to DCSs. Our numerical results in Fig. 4 show a strong dependence of the DCSs on the scattering and azimuthal angles, as well on the photon helicities of the two bicircular fields. For counter-rotating CP fields DCS is invariant to rotation around the z axis by an

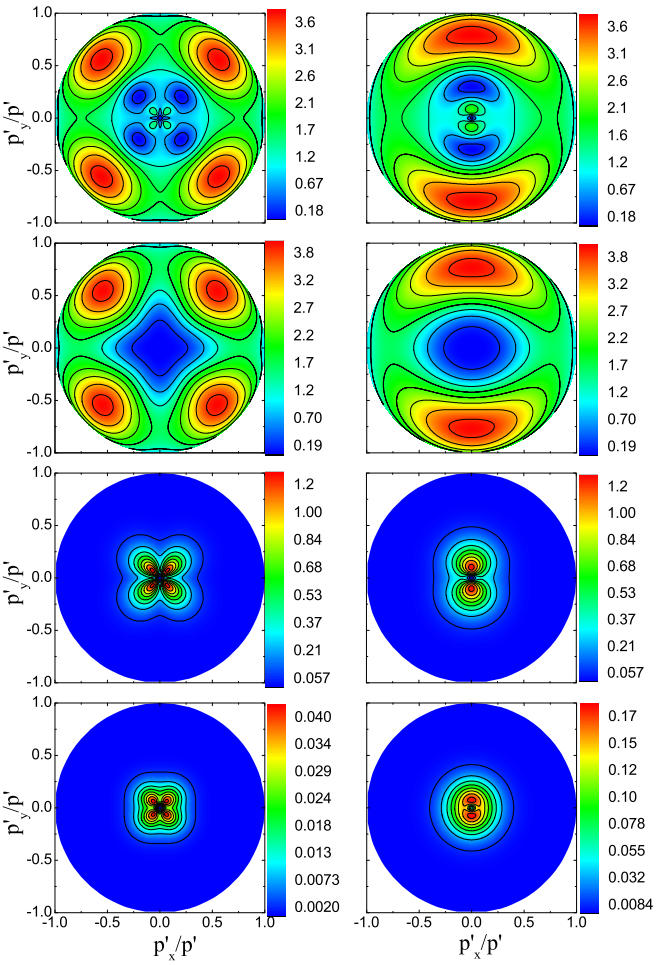

FIG. 4. Contour plots representing DCSs ($N = 2$), given by Eq. (11), for two-color left-handed CP fields in the right column and two-color left- and right-handed CP fields in the left column, as a function of the normalized Cartesian components of the projectile momentum vector in the polarization plane, p'_x/p' and p'_y/p'. The plots from top to bottom represent the total DCS, the projectile electron contribution calculated as $(2\pi)^4(p'/p)|T_2^{(0)}|^2$, the first-order atomic dressing contribution, $(2\pi)^4(p'/p)|T_2^{(1)}|^2$, and the second-order atomic dressing contribution $(2\pi)^4(p'/p)|T_2^{(2)}|^2$. The projectile electron energy is $E_p = 100$ eV, $\mathbf{p} \parallel \mathbf{e}_z$, the laser field intensities are $I_1 = I_3 = 1$ TW/cm^2, and the photon energies are $\omega_1 = 3$ eV and $\omega_3 = 3\omega_1$. The DCSs in a.u. are multiplied by a 10^4 factor and their magnitudes are indicated by the color scales in each row.

$\varphi = \pi/2$ azimuthal angle, whereas for corotating CP fields the corresponding azimuthal angle is $\varphi = \pi$. Both DCSs for co- and counter-rotating polarizations are symmetric with respect to reflection in the (x,z) and (y,z) planes, such that $d\sigma_2(\theta,\pi-\varphi)/d\Omega_{p'} = d\sigma_2(\theta,\pi+\varphi)/d\Omega_{p'}$ and $d\sigma_2(\theta,\pi/2-\varphi)/d\Omega_{p'} = d\sigma_2(\theta,\pi/2+\varphi)/d\Omega_{p'}$, respectively. Recently, similar rotational and reflection symmetries were obtained in the differential ionization rate in above-threshold ionization of krypton atoms by a two-color bicircular laser field of ω and 3ω frequencies [47].

For a better understanding of the contour plots presented in Fig. 4, we show in Fig. 5 the DCSs as a function of the scattering angle θ for two-color left-handed CP fields (corotating

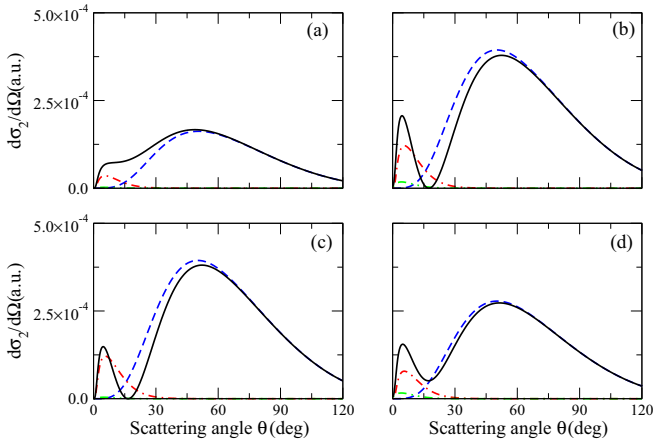

FIG. 5. The total two-photon DCSs (full lines) by two-color left- and right-handed-CP laser fields in panels (a) and (c) and two-color left-handed-CP laser fields in panels (b) and (d) as a function of the scattering angle θ. The azimuthal angles are $\varphi = 90^\circ$ in panels (a) and (b), $\varphi = 45^\circ$ in panels (c) and (d), and the rest of the parameters are the same as in Fig. 4. The dashed lines represent the projectile electron contribution calculated as $(2\pi)^4(p'/p)|T_2^{(0)}|^2$, while the dot-dashed and dotted lines represent the first- and second-order atomic dressing contributions, $(2\pi)^4(p'/p)|T_2^{(1)}|^2$ and $(2\pi)^4(p'/p)|T_2^{(2)}|^2$, respectively.

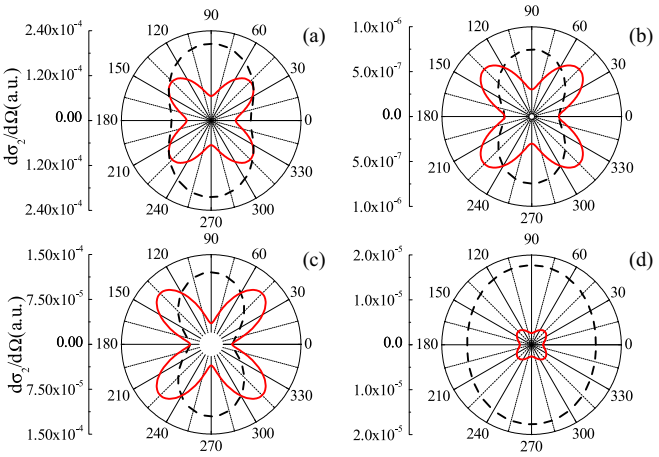

FIG. 6. Two-photon DCSs by two-color left- and right-handed-CP (full lines) laser fields and two-color left-handed-CP (dashed lines) laser fields are shown in panel (a) as a function of the azimuthal angle φ. The projectile electron contribution calculated as $(2\pi)^4(p'/p)|T_2^{(0)}|^2$ is plotted in panel (b), the first-order atomic dressing contribution $(2\pi)^4(p'/p)|T_2^{(1)}|^2$ is in panel (c), and the second-order atomic dressing contribution $(2\pi)^4(p'/p)|T_2^{(2)}|^2$ is in panel (d). The scattering angle is fixed at $\theta = 5^\circ$, and the rest of the parameters are the same as in Fig. 4.

case) in the right column and for left- and right-handed CP fields (counter-rotating case) in the left column. The DCSs are plotted at two azimuthal angles $\varphi = 90^\circ$ in Figs. 5(a) and 5(b), and $\varphi = 45^\circ$ in Figs. 5(c) and 5(d), while the other parameters concerning the scattering geometry, the field intensities, and the projectile and photon energies are the same as in Fig. 4. The dashed lines represent the projectile electron contribution to DCS calculated as $(2\pi)^4(p'/p)|T_2^{(0)}|^2$, while the dot-dashed and dotted lines represent the first- and second-order atomic dressing contributions given by $(2\pi)^4(p'/p)|T_2^{(1)}|^2$ and $(2\pi)^4(p'/p)|T_2^{(2)}|^2$, respectively. As expected from our theoretical calculations, the first-order laser-atom interaction is quite important at small scattering angles $\theta < 20^\circ$. By contrast, at larger scattering angles ($\theta > 20^\circ$) the projectile electron contribution to DCS is dominant due to nuclear scattering and determines the angular distribution of the two-photon DCS, as is shown by the dashed lines in Fig. 5. The projectile electron is scattered with the highest probability at scattering angles $\theta \simeq 50^\circ$ in Figs. 5(a) and 5(c), and $\theta \simeq 52^\circ$ in Figs. 5(b) and 5(d).

In order clarify the importance of the atomic dressing effect on the scattering signal presented in Fig. 4, we illustrate in Fig. 6(a) the two-photon DCSs in polar plots for counter-rotating (solid lines) and corotating (dashed lines) CP fields as a function of the azimuthal angle φ at the scattering angle $\theta = 5^\circ$, while the rest of the parameters are the same as in Fig. 4. The projectile contribution to DCS, $(2\pi)^4(p'/p)|T_2^{(0)}|^2$, is plotted in Fig. 6(b), while the first- and second-order atomic dressing contributions, calculated as $(2\pi)^4(p'/p)|T_2^{(1)}|^2$ and $(2\pi)^4(p'/p)|T_2^{(2)}|^2$, are depicted in Figs. 6(c) and 6(d), respectively. Because of the strong first- and second-order atomic dressing effects at small scattering angles, the atomic contribution is about 2 orders of magnitude larger compared to the projectile electron contribution. Moreover, at small scattering angles there is a clear enhancement of DCSs for corotating compared to counter-rotating CP fields and, obviously, the differences in magnitude between the DCSs for co- and counter-rotating polarizations originate from the different second-order atomic dressing terms, as is shown in the last row of Fig. 4 and Fig. 6(d). The two-photon DCS for corotating CP fields has a pattern profile predicted in the weak-laser-field regime by the $e^{-2i\varphi}$ term in Eq. (29), and the projectile electron is scattered with a high probability in the azimuthal angle directions $\varphi = \pi/2$ and $3\pi/2$. By contrast, the two-photon DCS for counter-rotating CP fields, as well as the electronic, first- and second-order atomic contributions to DCS, have a specific "four-leaf clover" pattern, as is analytically predicted in the weak-laser-field regime by the $e^{-4i\varphi}$ term in Eq. (30), and the projectile electron is scattered with a high probability in the azimuthal directions $\varphi = \pi/4, 3\pi/4, 5\pi/4$, and $7\pi/4$, as presented in Fig. 4. The two-photon DCS is invariant to rotation around the z axis by an azimuthal angle $\varphi = \pi$ for corotating CP fields and $\varphi = \pi/2$ for counter-rotating CP fields, and DCSs are symmetric with respect to reflection in the (x, z) and (y, z) planes for both co- and counter-rotating CP fields.

Finally, we present the DCSs for two-photon absorption in Figs. 7(a)–7(d) for co- and counter-rotating polarizations and the absolute values of the relative CDAD $|R(\varphi)|$, given by Eq. (21) in Figs. 7(e)–7(h), as a function of the azimuthal angle of the scattered electron. The scattering angle is fixed at the value $\theta = 5^\circ$ and the intensity of the third-harmonic laser is $I_3 = fI_1$, with the laser intensity ratios $f = 10, 1, 10^{-2}$, and 10^{-3} from top to bottom in Fig. 7, while the rest of the parameters are the same as in Fig. 4. For the harmonic field these laser parameters correspond to a quiver motion amplitude $\alpha_{03} = \alpha_{01}\sqrt{f}/9$ and an argument of the Bessel function

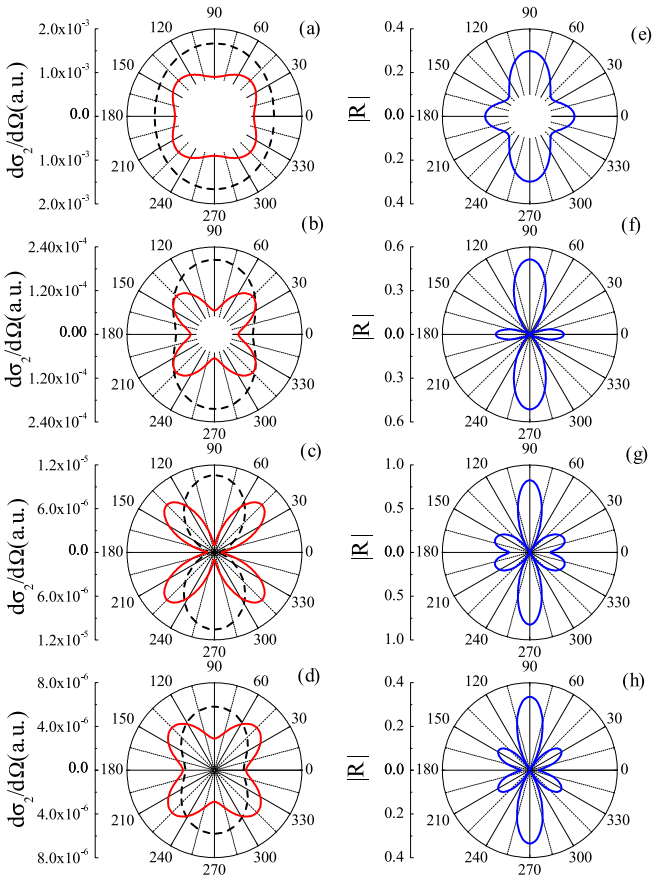

FIG. 7. The total two-photon DCSs in the left column and the absolute value of the relative CDAD, $|R(\varphi)|$, in the right column by two-color left- and right-handed-CP (full lines) laser fields and two-color left-handed-CP (dashed lines) laser fields as a function of the azimuthal angle φ. The scattering angle is fixed at $\theta = 5^\circ$, and intensities of the harmonic field I_3 are equal to $10I_1$ in panels (a) and (e), I_1 in panels (b) and (f), $10^{-2}I_1$ in panels (c) and (g), and $10^{-3}I_1$ in panels (d) and (h). The rest of the parameters are the same as in Fig. 4.

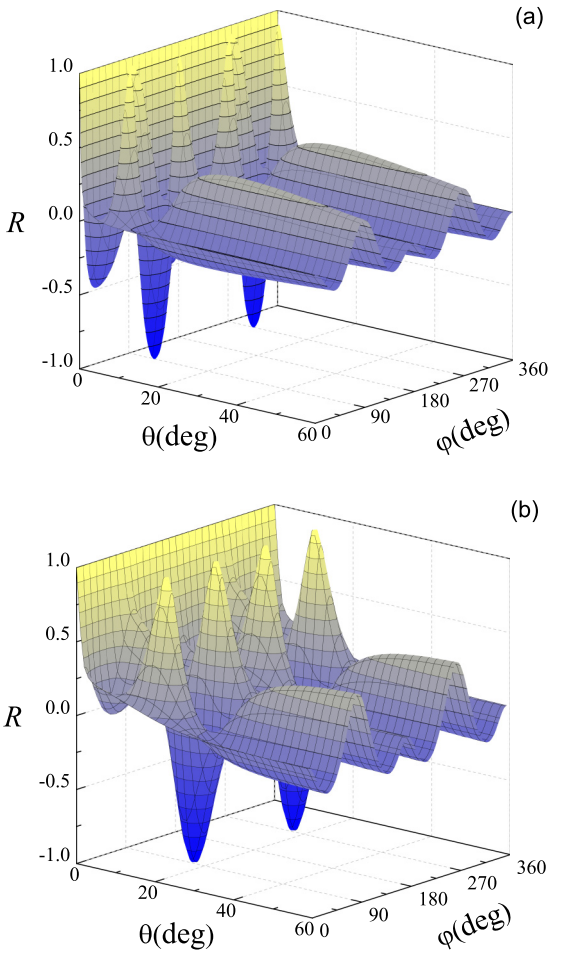

FIG. 8. Relative CDAD, $R(\theta, \varphi)$, as a function of the scattering and azimuthal angles for photon energies $\omega_1 = 1.5$ eV in panel (a) and $\omega_1 = 3$ eV in panel (b). The rest of the parameters are the same as in Fig. 4.

$\mathcal{R}_3 = \mathcal{R}_1\sqrt{f}/9$. At small scattering angles and relatively low intensities of the harmonic field, Figs. 7(b)–7(d), there is a strong dependence of DCSs on the azimuthal angle due to the first- and second-order atomic dressing terms for both co- and counter-rotating CP lasers, while at a higher intensity, $I_3 = 10I_1$ plotted in Figs. 7(a) and 7(e), there is a weaker dependence of DCSs on the azimuthal angle because of the dominance of the two different photon processes shown in Fig. 3(b). The absolute values of relative CDAD, $|R(\varphi)|$, are larger at the azimuthal angles $\varphi = \pi/2$ and $3\pi/2$ due to the different two- and fourfold symmetries of DCSs for co- and counter-rotating CP fields, as shown in Figs. 7(a)–7(d) and Figs. 7(e)–7(h). Therefore, at small scattering angles, because of the strong first- and second-order atomic dressing effects, there is a clear enhancement of DCSs for corotating compared to counter-rotating CP fields, as shown in Figs. 4 and 6, as well as an important dichroic effect.

We emphasize that the dichroic effect in DCS for two-photon absorption is not, however, a one-photon resonance effect, and it strongly depends on the atomic dressing by the bicircular laser field. We demonstrate this by comparing in Figs. 8(a) and 8(b) the three-dimensional numerical data for the relative values of the CDAD, $R(\theta, \varphi)$, calculated from Eq. (21) as a function of the scattering and azimuthal angles at two nonresonant photon energies, $\omega_1 = 1.5$ eV and $\omega_1 = 3$ eV. The other parameters are the same as in Fig. 4, namely, $E_p = 100$ eV and $I_1 = I_3 = 1$ TW/cm^2. For a clear view of the positive and negative values of relative CDAD, the same results of Figs. 8(a) and 8(b) are plotted as contour plots in Figs. 9(a) and 9(b). At $\omega_1 = 1.5$ eV the dichroic effect in DCS is as well very important but at relatively small scattering angles only, i.e., $\theta < 10^\circ$, where the atomic dressing dominates. By contrast, at $\omega_1 = 3$ eV there is a stronger dependence of the relative CDAD on both scattering and azimuthal angles because of the atomic dressing effects that occur at larger photon energies [41]. The dichroic effect is quite important at relatively small scattering angles $\theta < 25^\circ$ and is not negligible even at larger scattering angles. At small scattering angles, since the DCSs take very small values frequently due to the destructive interference between the projectile and atomic contributions, as depicted by the blue areas in the first row of Fig. 4, the relative CDAD oscillates quite rapidly between

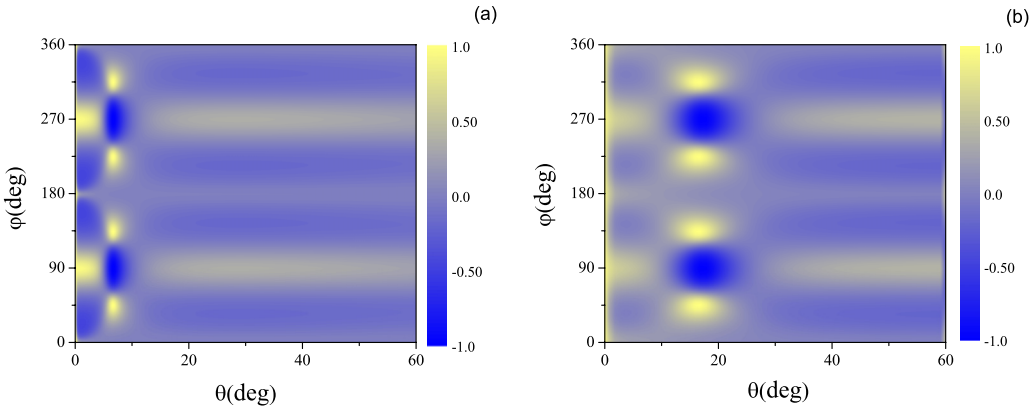

FIG. 9. Contour plots presenting the same results as in Fig. 8, namely, relative CDAD, $R(\theta, \phi)$, as a function of the scattering and azimuthal angles, θ and φ, for $\omega_1 = 1.5$ eV in panel (a) and $\omega_1 = 3$ eV in panel (b).

-1 and $+1$ in Figs. 8 and 9. Furthermore, as predicted from the closed formulas of DCSs for co- and counter-rotating CP fields, $d\sigma_N^{++}/d\Omega_{p'}$ or $d\sigma_N^{+-}/d\Omega_{p'}$ given by Eqs. (29) and (30), and Eqs. (33)–(35), at moderate laser intensities below 1 TW/cm^2 and larger scattering angles where the atomic dressing becomes negligibly small, namely, $\theta > 15^\circ$ for $\omega_1 = 1.5$ eV and $\theta > 40^\circ$ for $\omega_1 = 3$ eV, the dependence of the relative dichroism on the scattering and azimuthal angles in Figs. 8 and 9 is well described by Eq. (37).

IV. SUMMARY AND CONCLUSIONS

Using a semiperturbative method, we have theoretically studied the dichroic effect in electron-hydrogen scattering by a two-color bicircular laser fields of commensurate frequencies and moderate intensities. We have investigated a different regime of CD where the monochromatic components of the two-color CP field rotate in the same plane with the same or opposite helicities. We predict the existence of a nonlinear dichroic effect in DCS at high scattering projectile energies, which is sensitive to the photon energies and laser field intensities. We have derived useful analytical formulas for two-photon CDAD that give more physical insight into the scattering process and valuable information for experimental investigations. We stress that the analytical formulas obtained for co- and counter-rotating polarizations in the weak-laser-field limit, Eqs. (29) and (30), indicate that the two-photon DCSs are related to the interference of different quantum paths involving two photons with identical or different polarizations. By varying the intensity ratio of the co- and counter-rotating two-color CP laser field components we can manipulate the angular distribution of the scattered electrons. We have established that at UV photon energies and small scattering angles there is a clear enhancement of the DCS for corotating compared to counter-rotating laser fields because of the strong second-order atomic dressing effects. The dichroic effect in the angular distribution of scattered electrons originates from the nonzero atomic dressing at small scattering angles, whereas at large scattering angles the dichroic effect comes from the projectile contribution to the scattering signal.

In conclusion, the investigation of CDAD in the scattering signal is an effective method of studying the polarization effects in laser-assisted electron-atom collisions, and we hope that the dichroic effect discussed in the present paper will be useful in future theoretical and experimental studies.

ACKNOWLEDGMENTS

The work by G.B. was supported by research programs PN 16 47 02 02 through Contract No. 4N/2018 (Laplas V) and FAIR-RO Contract No. 01-FAIR/2016 from the UEFISCDI and the Ministry of Research and Innovation of Romania.

[1] K. W. Busch and M. A. Busch, *Chiral Analysis* (Elsevier, Amsterdam, 2006).
[2] G. Schönhense, Phys. Scr. **T31**, 255 (1990).
[3] M. Born and E. Wolf, *Principles of Optics* (Pergamon Press, London, 1991).
[4] H. Kleinpoppen, B. Lohmann, and A. N. Grum-Grzhimailo, *Perfect/Complete Scattering Experiments: Probing Quantum Mechanics on Atomic and Molecular Collisions and Coincidences* (Springer-Verlag, Berlin, 2013).
[5] N. A. Cherepkov, V. V. Kumetsov, and V. A. Verbitskii, J. Phys. B **28**, 1221 (1995).
[6] N. L. Manakov, A. Maquet, S. I. Marmo, V. Veniard, and G. Ferrante, J. Phys. B **32**, 3747 (1999).
[7] R. Taieb, V. Veniard, A. Maquet, N. L. Manakov, and S. I. Marmo, Phys. Rev. A **62**, 013402 (2000).
[8] P. Lambropoulos, Phys. Rev. Lett. **29**, 453 (1972).
[9] A. Cionga, F. Ehlotzky, and G. Zloh, Opt. Commun. **192**, 255 (2001).
[10] A. V. Flegel, M. V. Frolov, N. L. Manakov, A. F. Starace, and A. N. Zheltukhin, Phys. Rev. A **87**, 013404 (2013).
[11] J. Berakdar and H. Klar, J. Phys. B **26**, 3891 (1993); N. L. Manakov, S. I. Marmodag, and A. V. Meremianin, *ibid.* **29**, 2711 (1996); J. Berakdar, *ibid.* **32**, L27 (1999); J. Berakdar and H. Klar, Phys. Rep. **340**, 473 (2001).
[12] T. Mazza, M. Ilchen, A. J. Rafipoor, C. Callegari, P. Finetti, O. Plekan, K. C. Prince, R. Richter, A. Demidovich, C. Grazioli,

L. Avaldi, P. Bolognesi, M. Coreno, P. O'Keeffe, M. Di Fraia, M. Devetta, Y. Ovcharenko, V. Lyamayev, S. Düsterer, K. Ueda *et al.*, J. Mod. Opt. **63**, 367 (2016); T. Mazza, M. Ilchen, A. J. Rafipoor, C. Callegari, P. Finetti, O. Plekan, K. C. Prince, R. Richter, M. B. Danailov, A. Demidovich *et al.*, Nat. Commun. **5**, 3648 (2014).

[13] A. K. Kazansky, A. V. Grigorieva, and N. M. Kabachnik, Phys. Rev. A **85**, 053409 (2012); A. K. Kazansky, A. V. Bozhevolnov, I. P. Sazhina, and N. M. Kabachnik, J. Phys. B **47**, 065602 (2014).

[14] A. Cionga, F. Ehlotzky, and G. Zloh, Phys. Rev. A **61**, 063417 (2000).

[15] N. L. Manakov, S. I. Marmo, and V. V. Volovich, Phys. Lett. A **204**, 42 (1995).

[16] A. Cionga, F. Ehlotzky, and G. Zloh, Phys. Rev. A **62**, 063406 (2000); J. Phys. B **33**, 4939 (2000).

[17] M. O. Musa, A. MacDonald, L. Tidswell, J. Holmes, and B. Wallbank, J. Phys. B **43**, 175201 (2010).

[18] R. Kanya, Y. Morimoto, and K. Yamanouchi, Phys. Rev. Lett. **105**, 123202 (2010).

[19] B. A. de Harak, L. Ladino, K. B. MacAdam, and N. L. S. Martin, Phys. Rev. A **83**, 022706 (2011).

[20] Y. Morimoto, R. Kanya, and K. Yamanouchi, Phys. Rev. Lett. **115**, 123201 (2015); R. Kanya, Y. Morimoto, and K. Yamanouchi, in *Progress in Ultrafast Intense Laser Science X*, edited by K. Yamanouchi, G. Paulus, and D. Mathur (Springer, Cham, 2014), p. 1.

[21] N. J. Mason, Rep. Prog. Phys. **56**, 1275 (1993).

[22] F. Ehlotzky, A. Jaroń, and J. Z. Kamiński, Phys. Rep. **297**, 63 (1998).

[23] B. H. Bransden and C. J. Joachain, *Physics of Atoms and Molecules* (Longman, London, 1983).

[24] C. J. Joachain, N. J. Kylstra, and R. M. Potvliege, *Atoms in Intense Laser Fields* (Cambridge University Press, Cambridge, 2012), p. 466.

[25] A. Fleischer, O. Kfir, T. Diskin, P. Sidorenko, and O. Cohen, Nat. Photon. **8**, 543 (2014).

[26] C. A. Mancuso, D. D. Hickstein, P. Grychtol, R. Knut, O. Kfir, X. M. Tong, F. Dollar, D. Zusin, M. Gopalakrishnan, C. Gentry, E. Turgut, J. L. Ellis, M. C. Chen, A. Fleischer, O. Cohen, H. C. Kapteyn, and M. M. Murnane, Phys. Rev. A **91**, 031402(R) (2015).

[27] C. A. Mancuso, K. M. Dorney, D. D. Hickstein, J. L. Chaloupka, J. L. Ellis, F. J. Dollar, R. Knut, P. Grychtol, D. Zusin, C. Gentry, M. Gopalakrishnan, H. C. Kapteyn, and M. M. Murnane, Phys. Rev. Lett. **117**, 133201 (2016).

[28] S. Odžak and D. B. Milošević, Phys. Rev. A **92**, 053416 (2015).

[29] S. Odžak, E. Hasović, W. Becker, and D. B. Milošević, J. Mod. Opt. **64**, 971 (2017).

[30] F. Ehlotzky, Phys. Rep. **345**, 175 (2001).

[31] G. Buica, Phys. Rev. A **96**, 043419 (2017).

[32] G. Buica, J. Quant. Spectrosc. Radiat. Transf. **187**, 190 (2017).

[33] G. Buica, Phys. Rev. A **92**, 033421 (2015).

[34] D. M. Volkov, Z. Phys. **94**, 250 (1935).

[35] V. Florescu and T. Marian, Phys. Rev. A **34**, 4641 (1986).

[36] V. Florescu, A. Halasz, and M. Marinescu, Phys. Rev. A **47**, 394 (1993).

[37] F. W. Byron, Jr., and C. J. Joachain, J. Phys. B **17**, L295 (1984).

[38] N. F. Mott and H. S. W. Massey, *The Theory of Atomic Collisions* (Oxford University Press, London, 1965); C. Joachain, *Quantum Collision Theory* (North-Holland, Amsterdam, 1987).

[39] G. N. Watson, *Theory of Bessel Functions* (Cambridge University Press, Cambridge, 1962).

[40] S. Varró and F. Ehlotzky, J. Phys. B **28**, 1613 (1995).

[41] A. Cionga and G. Zloh, Laser Phys. **9**, 69 (1999).

[42] M. Gavrila and A. Costescu, Phys. Rev. A **2**, 1752 (1970).

[43] V. Veniard, M. Gavrila, and A. Maquet, Phys. Rev. A **35**, 448(R) (1987); A. A. Krylovetskiĭ, N. L. Manakov, S. I. Marmo, and A. F. Starace, J. Exp. Theor. Phys. **95**, 1006 (2002).

[44] N. L. Manakov, A. V. Meremianin, J. P. J. Carney, and R. H. Pratt, Phys. Rev. A **61**, 032711 (2000).

[45] M. Fifirig, V. Florescu, A. Maquet, and R. Taïeb, J. Phys. B **33**, 5313 (2000); M. Fifrig, A. Cionga, and F. Ehlotzky, Eur. Phys. J. D **23**, 333 (2003).

[46] A. Y. Istomin, E. A. Pronin, N. L. Manakov, S. I. Marmo, and A. F. Starace, Phys. Rev. Lett. **97**, 123002 (2006).

[47] E. Hasović, W. Becker, and D. B. Milošević, J. Phys.: Conf. Ser. **826**, 012009 (2017).